ChemPubSoc Europe

DOI: 10.1002/chem.201600218

CHEMISTRY A European Journal Full Paper

Nanotechnology

Two-Photon Excitation of a Plasmonic Nanoswitch Monitored by Single-Molecule Fluorescence Microscopy

Stefania Impellizzeri,[a] Sabrina Simoncelli,[a, c] Gregory K. Hodgson,[a] Anabel E. Lanterna,[a] Christopher D. McTiernan,[a] Françisco M. Raymo,[b] Pedro F. Aramendia,[c] and Juan. C. Scaiano*[a]

Abstract: Visible-light excitation of the surface plasmon band of silver nanoplates can effectively localize and concentrate the incident electromagnetic field enhancing the photochemical performance of organic molecules. Herein, the first single-molecule study of the plasmon-assisted isomerization of a photochrome-fluorophore dyad, designed to switch between a nonfluorescent and a fluorescent state in response to the photochromic transformation, is reported. The photochemistry of the switchable assembly, consisting of a photochromic benzooxazine chemically conjugated to a coumarin moiety, is examined in real time with total internal reflection fluorescence microscopy in the presence of silver nanoplates excited with a 633 nm laser. The metallic nanostructures significantly enhance the visible light-induced performance of the photoconversion, which normally requires ultraviolet excitation. The resulting ring-open isomer is strongly fluorescent and can also be excited at 633 nm. These stochastic emission events are used to monitor photochromic activation and show quadratic dependence on incident power. The utilization of a single laser wavelength for both photochromic activation and excitation effectively mimics a pseudo two-colours system.

Introduction

The utilization of surface plasmon resonance (SPR) of noble-metal nanoparticles (MNP) to manipulate light in the subwavelength regime with spatial and temporal control is of great interest, due to potential applications in nanoscaled lithography, data storage, and microscopy.[1] The SPR band is generated by the collective oscillation of free electrons upon interaction of the MNP with visible light. Conveniently, the shape and the spectral profile of the SPR band can be regulated by changing size, morphology, and surface coverage of the MNP.[2] When excited in the plasmon region, silver nanoparticles dramatically intensify the electromagnetic field and thus the photon flux experienced by molecules in the direct vicinity of the particles.[2b,3] This consequently amplifies the inherent spectroscopic and photochemical behavior of molecules in close proximity to the metal surface, improving the efficiency and the performance of photochemical reactions in the visible and NIR wavelength regime. Interestingly, photochromic transformations have been successfully exploited for tailoring, probing and monitoring SPR effects with convenient spectroscopic measurements.[4] Photochromic compounds switch reversibly between two isomeric states with distinct absorption spectra under optical control.[5] While photochromic transformations normally involve single-photon photoexcitation of the organic chromophore, the nanoparticle-mediated plasmonic enhancement of the electromagnetic field allows for the stimulation of multiphoton photochromic processes even at moderate illumination intensities, which would otherwise be inadequate for two-photon excitation.[6] In this context, nanoparticles can act as antennae, delivering excitation energy to molecules in close proximity to their surfaces. A number of examples have been reported, including a successful two-photon ring opening of diarylethenes.[4c,d] Since, however, these systems can only be monitored by absorption techniques, they are not amenable for single-molecule fluorescence microscopy studies.

Photochromic transformations can instead be designed to activate fluorescence under optical control, owing to the chemical engineering of the conjugation between a photochromic unit and an organic fluorophore.[7] As a consequence of the pronounced structural and electronic modifications associated with a photochromic transformation, the light-induced interconversion of the photochromic unit can be exploited to switch on the emission of the complementary fluorophore.

[a] *Dr. S. Impellizzeri, Dr. S. Simoncelli, G. K. Hodgson, Dr. A. E. Lanterna, C. D. McTiernan, Prof. J. C. Scaiano*
Department of Chemistry and Biomolecular Sciences, University of Ottawa
10 Marie Curie, Ottawa, Ontario K1N 6N5 (Canada)
E-mail: scaiano@photo.chem.uottawa.ca

[b] *Prof. F. M. Raymo*
Laboratory for Molecular Photonics, Department of Chemistry
University of Miami, 1301 Memorial Drive, Coral Gables, FL 33146-0431 (USA)

[c] *Dr. S. Simoncelli, Prof. P. F. Aramendia*
Centro de Investigaciones en Bionanociencias (CIBION) CONICET
Godoy Cruz 2390, Departamento de Química Inorgánica
Analítica y Química Física, FCEN, UBA, Pabellón 2
Ciudad Universitaria, Buenos Aires (Argentina)

Supporting information and the ORCID identification number(s) for the author(s) of this article can be found on the WWW under http://dx.doi.org/10.1002/chem.201600218.

The activation of fluorescence upon photochromic conversion offers the opportunity to apply single-molecule techniques, in which the photogenerated emission translates into a detectable signal for stochastic events at the single-molecule level.[8] For this study, we have selected the photochromic system shown in Figure 1. Upon ultraviolet illumination in acetonitrile, the 2*H*,4*H*-[1,3]benzooxazine ring in **1a** opens to generate the zwitterionic isomer **1b** on a subnanosecond timescale, where **1b** reverts to the original isomer **1a** (200 ns in acetonitrile. See

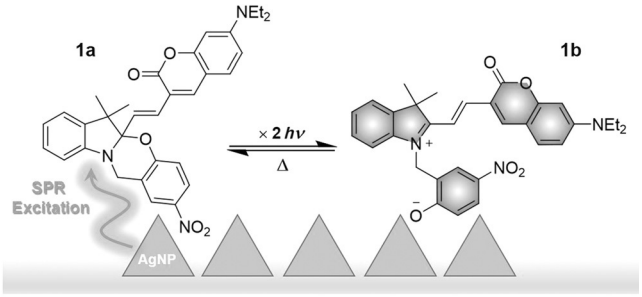

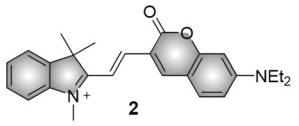

Figure 1. SPR-stimulated photochromic transformation of **1a** into **1b** and structure of the model cationic compound **2**.

laser flash photolysis experiments in Figures S11 and S12, Supporting Information).[9,10] The structural transformation of the photochrome brings the coumarin moiety into conjugation with the cationic fragment of the light-generated isomer and bathochromically shifts its absorption band by approximately 160 nm. As a result, the selective excitation of the newly generated absorption band centered at 580 nm allows the detection of the fluorescence of this species at 685 nm, which is readily observable following the photochromic transformation. Due to the short lifetime of their photogenerated isomer, the analysis of the photochromic transformation of benzooxazines is impossible by conventional stationary spectroscopic and analytical techniques. Nonetheless, the generation of an emissive isomer allows for monitoring of the photochromic conversion in real time, using total internal reflection fluorescence microscopy (TIRFM). The conversion of **1a** into **1b** normally requires excitation at wavelengths shorter than 450 nm, and is typically achieved using ultraviolet light. Herein, we used silver nanoplates (AgNP) in an attempt to establish whether the transformation shown in Figure 1 could instead be stimulated by excitation at 633 nm. Whereas compound **1a** is transparent at this wavelength, AgNP show strong plasmon absorption (Figure S1, Supporting Information). Furthermore, the transient absorption spectrum of **1b** (Figure S1, Supporting Information) shows that 633 nm is also a suitable excitation wavelength to observe fluorescence. This design allows both activation (the transformation of **1a** into **1b**) and excitation (of **1b**) to be conveniently achieved by the utilization of a single laser, simplifying the experimental setup and minimizing the associated cost. Our efforts were thus directed at the possibility of achieving fluorescence activation by the plasmon-mediated photochromic transformation of **1a**, as a consequence of the visible excitation of the SPR band of silver nanoplates (rather than the organic chromophore), and to exploit this process to detect emissive molecules. Results show that this transformation is indeed possible, and suggest a nonlinear process attributed to the plasmon-mediated enhancement of the performance of the photochromic transformation facilitated by the interaction of **1a** with the strong plasmonic field.

Results and Discussion

TIRFM samples consisted of a thin polymer layer of poly(methyl methacrylate) (PMMA) doped with **1a** and deposited over a monolayer of triangular shaped AgNP coated on a glass coverslip. SEM of the synthesized AgNP (Figure S2, Supporting Information) reveal triangular shaped nanocrystals with a size distribution of 90 ± 9 nm.

Relative to their spherical counterparts, triangular silver plates are known to generate stronger plasmonic fields, which are localized at the vertices of the prisms.[11] The formation of clusters of closely spaced nanoparticles can further enhance performance by constraining plasmon effects to the nanoscaled gaps between the vertices.[12] The AgNP monolayer was prepared by using (3-aminopropyl)triethoxysilane (APTES) as a coupling agent. AFM images of the substrates show the presence of large AgNP agglomerates as well as complete surface coverage of the substrate (Figure S3, Supporting Information). A solution of **1a** in poly(methyl methacrylate) was then spin-coated atop the functionalized slides in order to obtain polymer films approximately 100 nm thick. The construction and the preparation of the sample ensures that molecules dispersed atop the AgNP monolayer will be in close proximity to the enhanced field produced by excitation of the localized surface plasmon of AgNP, with the gaps between the densely packed nanostructures filled by polymer.[13] With full coverage of the slide with AgNP and a polymer film 100 nm thick, the enhanced field is expected to cover roughly 20% of the sample.[14] This ensures that most molecules of **1a** will be sufficiently close to AgNP and within the field enhancement region. A fraction of the small population of **1b** in thermal equilibrium with **1a** will experience field enhancement. TIRFM imaging and analysis of a PMMA solution of **1a** spin-coated atop a AgNP monolayer after 633 nm excitation at full laser power density (83 W cm^{-2}) reveals a significant increase in the mean fluorescence intensity (Figure 2a) as well as in the number of detected events with respect to **1a** imaged in the absence of the AgNP (Figure 2b; see the Supporting Video 1). For an immediate visual comparison, Figure 2 displays the contrast between two regions of a coverslip, in which only one of them is functionalized with AgNP. The plasmon-induced enhancement of the fluorescence intensity allows for improved detection of bursting events with higher signal-to-noise ratio (Figure 2a, left panel) compared with nonenhanced molecules

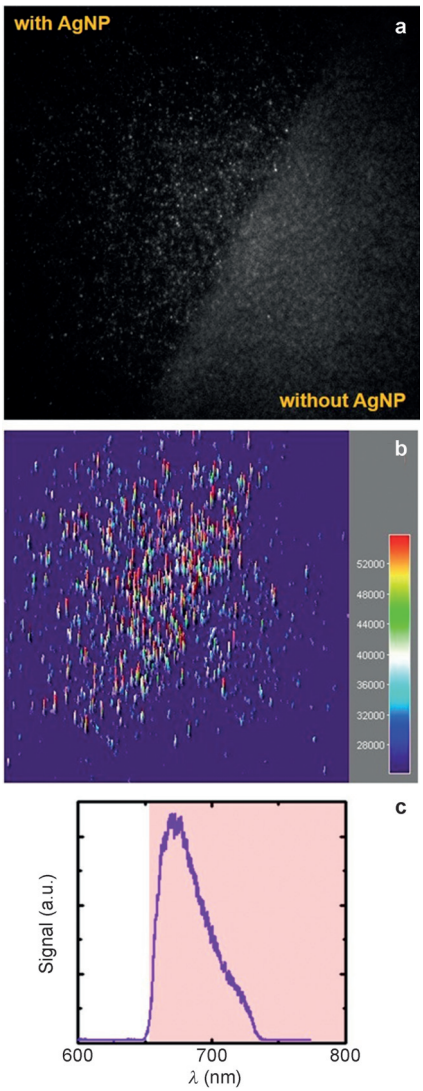

Figure 2. Single frame (a) and 3D representation (b, the color bar indicates the intensity of the bursting events) (100 frames/image sequence, integration time per frame = 999 ms) of a PMMA film doped with **1a** (10^{-6} mol kg^{-1} polymer) recorded upon illumination with a CW laser operating at 633 nm over a cover glass in which roughly the left half is functionalized with AgNP. Emission spectrum (c) of the fluorescent bursts measured with an Andor spectrograph.

(Figure 2a, right panel). Although small populations of fluorescent molecules are evident even in the absence of AgNP, as a consequence of spontaneous thermal activation due to the equilibrium between the closed (**1a**) and the open form (**1b**), the three-dimensional projection of the same sample provides immediate visual confirmation of a significant increase in the number of bursting events (Figure 2b). The emission spectrum of such bursting events confirmed that they indeed correspond to emission from **1b**, as shown in Figure 2c.

AgNP monolayers on a glass coverslip are highly scattering under the selected experimental conditions. The background scattering from AgNP, measured by imaging PMMA spin-coated atop the nanostructures, was systematically analysed at different excitation powers in order to evaluate possible interference in identifying actual events of interest. The temporal intensity profiles for representative background trajectories are shown in Figure S4 (Supporting Information). Although the average base intensity of each scattering trajectory may vary according to the non-uniform distribution of the nanoparticles (NP) on the glass surface, on the timescale of the experiment (100 s, Figure S4, Supporting Information) it remains approximately constant for a given laser power, and in no cases were bursting signals or sharp jumps in intensity observed. Indeed, analysis of residuals of the scattering profiles (Figure S5, Supporting Information) show that the variance is normally distributed, which confirms the normality of the background signals over time. In contrast, analysis of the variance of the residuals for intensity trajectories extracted from the TIRFM image sequences corresponding to PMMA films containing **1a** (10^{-6} mol kg^{-1} pol) spin-coated atop AgNP shows numerous instances of substantial drift from linear behavior. This phenomenon is indicative of the presence of bursting events in an intensity trajectory. Since this method considers only the absolute drift in the variance, real bursting events are identified independent of their intensities, and can thus be detected even in cases where scattering from dense clusters of NP precludes the intensity-based identification of the emission of a few single molecules directly atop the NP. Being completely independent of relative profile intensities, this method relies upon the absolute drift in signal variance in order to identify trajectories containing valid bursting events, which are immediately detected, while scattering profiles are excluded from further analysis. To better illustrate the validity of the analysis, a representative example is reported in Figure S6 (for scattering) and Figure S7 (for a bursting event) of the Supporting Information. Indeed, the protocol described allows for rapid, streamlined identification of ROIs that contain potential bursting events by permitting a preliminary screening of thousands of trajectories in a fraction of the time that would be required for manual burst identification, and with significantly greater accuracy. However, manual visual examination of the individual traces making up the pool of trajectories remaining after the screening process was still necessary in order to identify trajectories containing multiple bursting events (Figure S8a) and to confirm that each and every bursting event contained within these trajectories was valid. That is, trajectories affected by camera artifacts or the presence of dust particles on the optics or sample surface could potentially pass the automated screening test if any of these effects resulted in a substantial drift to the variance of the residual. Such trajectories were excluded from further analysis, and any apparent bursting events in which the entire duration of the burst was not observed from start to finish were also discarded (Figures S8b and S8c, Supporting Information).

Once the procedure described above had been applied, the actual bursting events were manually counted. The number of counted events as a function of the power of the exciting laser for compounds **1a** and **2** in the presence of AgNP, as well as for compound **1a** in the absence of the MNP, is illustrated in Figure 3 and Table S1 (Supporting Information). Control experiments (compound **1a** in the absence of AgNP and compound

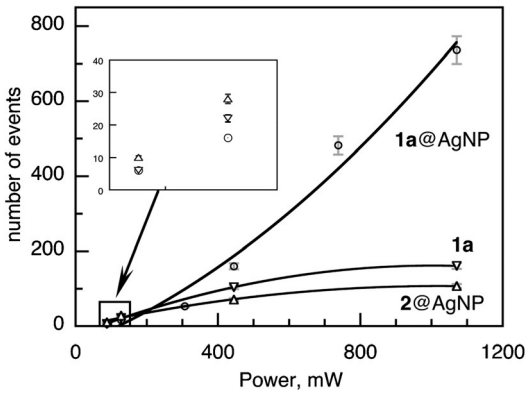

Figure 3. Number of counted events as a function of the power of the exciting laser for PMMA films doped with compounds **1a** or **2** in the presence of AgNP and compound **1a** in the absence of AgNP, recorded upon illumination with a CW laser operating at 633 nm (100 frames/image sequence, integration time per frame = 999 ms). The errors are estimated as ±2 events or 5%, whichever is larger. The quadratic fits are simply to help visualize the data and is only meaningful in the case of **1a**@AgNP. 100% of the laser power corresponds to 2231 mW.

2 in the presence of AgNP) were performed by imaging samples at 4, 6, 20 and 48% of full laser power, while for the investigation of compound **1a** in the presence of AgNP intermediate excitation powers were also included.

From the results illustrated in Figure 3 and Table S1, Supporting Information, it is clear that the number of detected fluorescent bursts attributed to **1b** in the presence of AgNP is significantly higher than the number observed for the compound imaged in the absence of AgNP. In principle, this remarkable behavior could be the result of: 1) nanoparticle-induced enhancement of the emission intensity of the small population of **1b** present in equilibrium with **1a** (i.e. events are detected more easily due to enhancement of the fluorescence); 2) thermally activated transformation of **1a** to **1b** by plasmonic heating; or 3) the ability of the AgNP to promote the formation of **1b** upon excitation of the SP band through a two-photon process.

To rule out the first hypothesis, we conducted control experiments by imaging a solution of compound **2** in PMMA spin-coated atop AgNP. Indeed, the degree of enhancement of the fluorescence in the presence of the nanostructures depends on the relative fluorophore–nanoparticle distance.[3a,15] Nonetheless, compounds **2** and **1b** share the same chromophore and thus the analysis of **2** atop AgNP provides reliable evidence of the expected enhancement for **1b** atop AgNP at the same laser power (Figure S9, Supporting Information). However, the dependence of the number of events on the power of the exciting laser differs significantly from a sample comprising **1a** atop AgNP in PMMA. Double logarithmic plots (Figure 4) show that the dependence of number of bursting events on the excitation power for films of **1a** in the presence of AgNP has a slope *m* of 2.0 (Figure 4a). In contrast, compound **2** spin-coated atop AgNP (Figure 4c) shows a dependence closer to a slope *m* of 1, albeit with some curvature in the plot, similar also to the film doped with **1a** in the absence

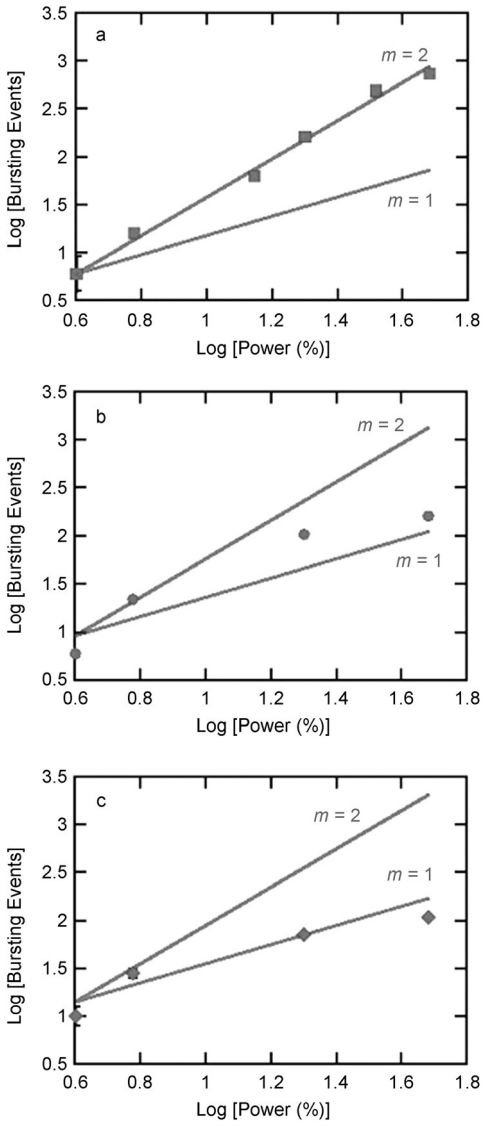

Figure 4. Logarithmic plots of the number of detected bursting events (100 frames/image sequence, integration time per frame = 999 ms) for PMMA films doped with compounds **1a** (a) in the presence of AgNP, compound **1a** in the absence of AgNP (b) and **2** in the presence of AgNP (c), recorded upon illumination with a CW laser operating at 633 nm. The errors are estimated as ±2 events or 5%, whichever is larger. For *x*-axis values larger than 1, the errors are within the dimensions of the point drawn; some of these are more readily visualized in Figure 3.

of the nanostructures (Figure 4b); the partial curvature of the plots is likely caused by partial saturation of the excitable chromophores at the highest energies used. This behaviour indicates that only in the case of **1a**@AgNP there is a clear nonlinear dependence corresponding to a two-photon process, also justifying the use of a parabola for this specific system in Figure 3. These data demonstrate that the nanoplates promote the transformation of a significant population of **1a** into **1b** upon excitation of the SP band at 633 nm. The value of the slope together with the lack of absorbance of **1a** at 633 nm (Figure S1, Supporting Information) shows that two-photon excitation at 633 nm, promoted by the stimulation of the surface plasmon band of AgNP at the same wavelength, is responsible

for improving the performance of the photochromic transformation of **1a** into **1b**.

Our second hypothesis above involves the possibility of thermal activation of **1a**. The area in close proximity to the surface of MNP can reach high temperatures upon excitation of the plasmon band.[16] To evaluate whether the ring-opening reaction (**1a**→**1b**) could be due to thermal stimulation, we prepared thin PMMA films of **1a** deposited over coverslips functionalized with spherical gold nanoparticles (AuNP, 80 nm in diameter) and recorded TIRFM image sequences upon excitation of the AuNP plasmon band at 543 nm (Figure S10, Supporting Information). Compound **1b** also absorbs at 543 nm (Figure S1, Supporting Information) and thus can also be excited at this wavelength in order to detect its fluorescence. Due to the impracticality of physically heating the microscope objective at high temperatures without seriously damaging the equipment, the AuNP based system was chosen as a reliable model to test whether the isomerization was photochemically or thermally driven. Indeed, the local field enhancement produced by spherical AuNP is significantly smaller than for AgNP with triangular geometry[11–12,17] and, therefore, a plasmon-assisted two-photon isomerization process would be unlikely. However, light-to-heat conversion remains highly effective.[18] It should be noted that the parameters for this study require careful selection of experimental conditions. The use of a different material (gold vs. silver), a different laser excitation wavelength, and different plasmonic properties are all important considerations in the quantification of the heating by gold and silver nanostructures. However, most of these parameters are readily available or easy to estimate (see the Supporting Information). In this case, we have concluded that 80 nm AuNP excited at 543 nm provides a reasonable comparison to evaluate the possible contribution of plasmonic heating to the **1a**→**1b** interconversion. According to our calculations, the heat generated by excitation of spherical AuNP at 543 nm using 100% of the laser power is comparable to that generated by excitation of AgNP at 633 nm at 15.7% of excitation capacity (see the Supporting Information). Using the power settings available at 633 nm, we detected 63 events for polymer films doped with **1a** and spin-coated atop AgNP at 14% of the total excitation power at $\lambda_{ex}=633$ nm and 160 events at 20% power (Table S1, Supporting Information). If the experimental observations in Figure 4a resulted from significant thermal activation, then imaging of samples of **1a** in PMMA spin-coated atop AuNP should provide a number between 63–160 events. The same protocol for counting bursting events described above was applied. By exclusively monitoring the absolute drift in the variance of the signals, the identification of bursting events remained independent of their intensities. Therefore, SPR enhancement (whether due to AuNP or AgNP) of the emission of **1b** did not affect single-molecule detection. As was done for AgNP, this was also confirmed by imaging compound **2** atop AuNP. However, we detected only nine events attributable to **1b** atop AuNP. Therefore, the heat generated upon excitation of the SP of AgNP is insufficient for promoting the conversion of **1a** into **1b**. After having eliminated nanoparticle-induced enhancement of emission and thermal activation as possible causes for the light-induced **1a**→**1b** conversion, the only reasonable explanation remains that AgNP are able to promote the formation of **1b** through a two-photon process mediated by laser excitation of the surface plasmon band of AgNP in the visible region in which **1a** has no absorption.

Conclusion

We have demonstrated that visible-light excitation of the surface plasmon band of AgNP improves the performance of an activatable photochromic dyad that is transparent in the visible region. In the presence of AgNP, a photoinduced photochromic isomerization that normally requires ultraviolet irradiation (**1a**→**1b**) can be performed with moderate excitation powers using a simple experimental setup. Results indicate that AgNP effectively promote two-photon excitation, and consequently enhance the fluorescence activation of the switchable probe. Our approach demonstrates that even with photochromic systems that do not display any photochemical activity under visible-light illumination, the use of plasmon-enhanced fields can improve performance and allow real-time monitoring of the dynamic process using single-molecule fluorescence microscopy.

Experimental Section

Materials

Silver nanoplates (AgNP) were prepared according to literature protocols.[4] Specifically, silver seeds were obtained by 5 min UVA illumination of an aerated solution of 0.2 mM Irgacure 2959, 0.2 mM $AgNO_3$ and 1 mM trisodium citrate in a Luzchem photoreactor. The growth from nanoparticles to nanoplates was performed by illuminating an oxygenated solution of the seeds with 590 nm air-cooled LEDs for 24 h. SEM images were acquired with a JEOL JSM-7500F field-emission scanning electron microscope. Gold nanoparticles (AuNP) were prepared with a growth seed method according to literature protocol.[19] Compounds **1a** and **2** were synthesized by following literature procedures.[9b]

Methods

Solvents were purified with a LC Technology Solutions Inc. SPBT-1 Bench Top Solvent Purification System. Chemicals were purchased from Sigma–Aldrich or Fisher Scientific. All the reactions were monitored by thin-layer chromatography, using aluminum sheets coated with silica (60, F254). NMR spectra were recorded at room temperature with a Bruker Avance 300 spectrometer. Mass spectral analysis was performed with a 6890N Network GC System equipped with a 5973 Mass Selective Detector from Agilent Technologies. ESI mass spectra in positive mode were acquired with a Micromass Q-TOF I mass spectromter. High-resolution EI mass spectra were acquired with a HRes, Concept S1, Magnetic Sector mass spectrometer and were conducted in the John L. Holmes Mass Spectrometry Facility at the Department of Chemistry and Biomolecular Sciences, University of Ottawa. Absorbance and emission spectra were recorded using a Cary 50 UV/Vis spectrophotometer and a PTI spectrofluorometer, respectively, using a quartz cuvette with a path length of 1 cm. Laser flash photolysis was performed with a Q-switched Nd:YAG-laser (355 nm, 10 mJ/pulse) in a LFP-111 system (Luzchem Research Inc., Ottawa, Canada), in 1×

1 cm LFP-Luzchem cuvettes or glass slides (Fisher Scientific); the absorbance of the samples at 355 nm was ~0.3. Laser flash photolysis with 630 nm excitation were performed with Surelite plus OPO (5 mJ); solutions were prepared as 3 mL samples in a 1% PMMA solution in MeCN with the absorbance of **1a** being 0.2 at 415 nm. Upon addition of 100 μL of AgNP the absorbance of the solution was 0.01 at 630 nm.

Single-molecule imaging and analysis

Single-molecule fluorescence experiments were performed within thin poly(methyl methacrylate) (PMMA) films containing the photochrome-fluorophore assembly **1a** deposited over AgNP-functionalized glass coverslips. All glassware (vials, pipets and coverslips) for single-molecule experiments were cleaned with piranha solution (H_2O_2/H_2SO_4 1:3) for 1 h and then rinsed thoroughly with MilliQ water. The slide surface was functionalized with APTES by immersing the coverslips in a 2% v/v aqueous APTES solution for 2 h, then washing in an ultrasound bath with MilliQ water, and drying under a nitrogen flow. The nanoparticle monolayer was obtained by adding a drop of concentrated AgNP solution to the coverslip, rinsing after 1 h with water and then drying with nitrogen. Polymer films were spin-coated (2500 rpm, 45 s) from a 1% w/w PMMA solution in acetonitrile containing **1a** or **2** (10^{-6} mol kg^{-1} pol) onto the functionalized coverslips. AFM imaging was performed under air using a Molecular Imaging PicoPlus AFM working in noncontact mode, using AFM probes from Budget Sensors (Tap150-G) with a nominal resonance frequency of 150 kHz (force constant of 5 N m^{-1}). Fluorescence imaging was performed with an Olympus FV1000 TIRF microscope (Olympus, Japan) equipped with He-Ne CW lasers (633 nm, 05-LHP-991 and 543 nm, 05-LGP-193) and an EM-CCD (Rolera EM-C2, Q-Capture). The Olympus FV1000 is also coupled to a Fluorescence Lifetime Imaging (FLIM) system (MicroTime 200, PicoQuant, Germany). A beam splitter cube was used to reflect the excitation light into the oil immersion TIR (Total Internal Reflection) objective (100X, N.A. 1.45, Olympus, PLAPO). The fluorescence emission collected was in the spectral range of 655–725 nm. The laser power density at the sample was measured at 83 W cm^{-2} at 100% of the laser power at $\lambda_{ex}=633$ nm, and 26 W cm^{-2} at $\lambda_{ex}=543$ nm. Each frame of the TIRFM image sequences recorded consists of a 501×502 pixel (px), 80×80 μm image with a pixel size of 159 nm. Fluorescence spectra of stochastic emission (bursting events) were recorded with the coupled FLIM system, equipped with a frequency doubled picosecond pulse diode laser (637 nm, 100 ps, 40 MHz, LDH-P-FA-530 L, PicoQuant). The laser beam was collimated and focused through a fiber-coupling unit. A beam splitter Z638rdc (Chroma) was used to reflect the excitation light into the oil immersion TIR objective. The epifluorescent signal was passed through a 560 nm long pass filter and collected by a Shemrock SR-163 spectrograph (Andor Technology, South Windsor, USA). Analysis of TIRFM image sequences (100 frames/image sequence, integration time per frame = 999 ms) was carried out using a combination of ImageJ (NIH), MATLAB (MathWorks) and OriginLab software. In brief, 3×3 px regions of interest (ROIs) were selected based on the automated identification of stochastic emission representing the formation of **1b**. After background subtraction was performed with ImageJ (rolling ball algorithm) bursting events were examined graphically. This was done by first using ImageJ to measure the mean fluorescence intensity inside each ROI for every frame in a 100 s image sequence. The data were tabulated and imported into OriginLab, where frame numbers were converted to units of time. Mean intensity was then plotted as a function of time to generate unique intensity profiles for every ROI. Graphical residual analysis was then performed in order to identify fluorescence bursting events, which are characterized by a variance of the signal residual exceeding the positive limit of the variance exhibited by a distribution of residuals representing scattering by AgNP only (Figure S6; compare with Figure S7, Supporting Information). The latter was obtained from TIRFM imaging of PMMA spin-coated atop AgNP in the absence of **1a**, **1b**, or **2**. Further details on this protocol are available in the Supporting Information.

Acknowledgements

We acknowledge financial support from the Natural Sciences and Engineering Research Council of Canada, Canada Research Chairs and Canadian Foundation for Innovation. S. Impellizzeri acknowledges the award of a Banting Postdoctoral Fellowship. S. Simoncelli acknowledges a travel grant from UBA and a PhD fellowship from CONICET as well as a DFAIT (Canada) fellowship from ELAP (Emerging Leaders in the Americas Program). G. K. Hodgson acknowledges the award of an Ontario Graduate Scholarship. P. F. Aramendia is a staff member of CONICET (Carrera del Investigador Científico, Consejo Nacional de Investigaciones Científicas y Técnicas, Argentina).

Keywords: nanoparticles · photochromes · surface plasmon · TIRFM

[1] W. L. Barnes, A. Dereux, T. W. Ebbesen, *Nature* **2003**, *424*, 824–830.
[2] a) K. L. Kelly, E. Coronado, L. L. Zhao, G. C. Schatz, *J. Phys. Chem. B* **2003**, *107*, 668–677; b) E. Hao, G. C. Schatz, *J. Chem. Phys.* **2004**, *120*, 357–367; c) K. Stamplecoskie, J. C. Scaiano, *J. Am. Chem. Soc.* **2010**, *132*, 1825–1827; d) K. Stamplecoskie, J. C. Scaiano, *Photochem. Photobiol.* **2012**, *88*, 762–768.
[3] a) P. Anger, P. Bharadwaj, L. Novotny, *Phys. Rev. Lett.* **2006**, *96*, 113002; b) P. K. Jain, M. A. El-Sayed, *Chem. Phys. Lett.* **2010**, *487*, 153–164.
[4] a) H. Nishi, T. Asahi, S. Kobatake, *J. Phys. Chem. C* **2009**, *113*, 17359–17366; b) R. Klajn, P. J. Wesson, K. J. M. Bishop, B. A. Grzybowski, *Angew. Chem. Int. Ed.* **2009**, *48*, 7035–7039; *Angew. Chem.* **2009**, *121*, 7169–7173; c) Y. Tsuboi, R. Shimizu, T. Shoji, N. Kitamura, *J. Am. Chem. Soc.* **2009**, *131*, 12623–12627; d) B. Wu, K. Ueno, Y. Yokota, K. Sun, H. Zeng, H. Misawa, *J. Phys. Chem. Lett.* **2012**, *3*, 1443–1447.
[5] J. C. Crano, R. J. Guglielmetti, *Organic Photochromic and Thermochromic Compounds*, Plenum Press, New York, **1999**.
[6] J. R. Lakowikz, *Principles of Fluorescence Spectroscopy*, Springer, New York, **2006**.
[7] J. Cusido, S. Impellizzeri, F. M. Raymo, *Nanoscale* **2011**, *3*, 59–70.
[8] G. Baffou, R. Quidant, F. J. García de Abajo, *ACS Nano* **2010**, *4*, 709–716.
[9] a) E. Deniz, M. Tomasulo, J. Cusido, I. Yildiz, M. Petrella, M. L. Bossi, S. Sortino, F. M. Raymo, *J. Phys. Chem. C* **2012**, *116*, 6058–6068; b) E. Deniz, S. Sortino, F. M. Raymo, *J. Phys. Chem. Lett.* **2010**, *1*, 3506–3509.
[10] The kinetic analysis of the isomerization is discussed in the Supporting Information.
[11] H. Nabika, M. Takase, F. Nagasawa, K. Murakoshi, *J. Phys. Chem. Lett.* **2010**, *1*, 2470–2487.
[12] a) A. Sundaramurthy, P. J. Schuck, N. R. Conley, D. P. Fromm, G. S. Kino, W. E. Moerner, *Nano Lett.* **2006**, *6*, 355–360; b) K. Ueno, S. Juodkazis, V. Mizeikis, K. Sasaki, H. Misawa, *Adv. Mater.* **2008**, *20*, 26–30; c) R. Alvarez-Puebla, L. M. Liz-Marzán, F. J. García de Abajo, *J. Phys. Chem. Lett.* **2010**, *1*, 2428–2434; d) X.-Y. Zhang, A. Hu, T. Zhang, W. Lei, X.-J. Xue, Y. Zhou, W. W. Duley, *ACS Nano* **2011**, *5*, 9082–9092.
[13] S. Simoncelli, M. J. Roberti, B. Araoz, M. L. Bossi, P. F. Aramendía, *J. Am. Chem. Soc.* **2014**, *136*, 6878–6880.
[14] In the case of a 90 nm spherical nanostructure, the volume where the field is higher than half of the intensity at the NP surface is approximately a cilinder of 20 nm in height and 90 nm in diameter, located at

each side of the NP in the direction defined by the incident photon polarization.

[15] A. Wokaun, H. P. Lutz, A. P. King, U. P. Wild, R. R. Ernst, *J. Chem. Phys.* **1983**, *79*, 509 – 514.

[16] A. O. Govorov, H. H. Richardson, *Nano Today* **2007**, *2*, 30 – 38.

[17] a) W. Wenseleers, F. Stellacci, T. Meyer-Friedrichsen, T. Mangel, C. A. Bauer, S. J. K. Pond, S. R. Marder, J. W. Perry, *J. Phys. Chem. A* **2002**, *106*, 6853 – 6863; b) M.-Q. Zhu, G.-F. Zhang, C. Li, M. Aldred, E. Chang, R. A. Drezek, A. D. Q. Li, *J. Am. Chem. Soc.* **2011**, *133*, 365 – 372.

[18] a) O. Neumann, A. D. Neumann, E. Silva, C. Ayala-Orozco, S. Tian, P. Nordlander, N. J. Halas, *Nano Lett.* **2015**, *15*, 7880 – 7885; b) C. Fasciani, C. J. B. Alejo, M. Grenier, J. C. Netto-Ferreira, J. C. Scaiano, *Org. Lett.* **2011**, *13*, 204 – 207.

[19] K. L. McGilvray, M. R. Decan, D. Wang, J. C. Scaiano, *J. Am. Chem. Soc.* **2006**, *128*, 15980 – 15981.

Received: January 16, 2016
Published online on April 8, 2016